Dynamical equilibrium between magnetic ions and photocarriers in low Mn-doped single quantum dots

T. Clément, D. Ferrand,* L. Besombes, H. Boukari, and H. Mariette
CEA-CNRS Group "Nanophysique et Semiconducteurs," Institut Néel, CNRS–Université J. Fourier, 25 rue des Martyrs, BP 166, 38042 Grenoble Cedex 9, France

(Received 27 November 2009; revised manuscript received 23 February 2010; published 30 April 2010)

For low Mn-doped Cd(Mn)Te/ZnTe single quantum dots, we report a nonlinear behavior of exciton energy as a function of magnetic field, which differs from the usual giant Zeeman effect. This effect is modeled by a positive feedback loop in the heating process of Mn spins by carriers photocreated in the vicinity of the dot. It results in a highly nonlinear and magnetic field dependent Mn spin heating process. This effect prevails when dealing with magnetic dot deposited on a thin two-dimensional layer and containing about 1% Mn. This shows that controlling the coupling between the magnetic dot and its local environment is a corner stone to achieve nanoscale spin manipulation.

DOI: 10.1103/PhysRevB.81.155328 PACS number(s): 75.75.−c, 71.35.Ji, 75.50.Pp, 78.67.Hc

I. INTRODUCTION

Magnetic doping of semiconductor quantum dots (QDs) opens new possibilities for the development of nanoscale spintronic devices. Since controlling the magnetic doping at a level of a single Mn atom in QDs has been demonstrated,[1,2] the interest in this field is expanding rapidly. Theoretical studies suggest that the magnetic order in such QDs could be tailored by the number of confined carriers, the QD geometry, the position and the number of magnetic ions.[3,4] Moreover, the interaction of the QD with its local environment is essential and has to be taken into account as it was demonstrated in various QDs (see for example Refs. 5 and 6). Here, we show that in the case of magnetic QDs, Mn spin dynamics is very sensitive to the exchange coupling with free carriers moving in the wetting layer (WL) underneath the QDs.

The critical role played by the coupling between free carriers and Mn spins has been first demonstrated in magnetic quantum wells (QWs).[7,8] Two-dimensional (2D) carrier diffusion leads to thermal instabilities with spontaneous formation of hot and cold spin domains.[9,10] In QWs, the thermal properties of Mn spins are strongly affected under magnetic field as revealed by the observation of non Brillouin giant Zeeman effect.[11]

Compared to these 2D systems, a single QD is used in this work as a local probe to get rid of any spatial fluctuations and to reveal the energy and spin transfer from photocreated carriers to Mn spins. We will show that, in such strongly confined system, a nonlinear spin carrier coupling dominates all the magneto-optical properties. This coupling is enhanced by the large spatial confinement of the thin WL.

For low Mn doped QDs, we observe strong deviations from Brillouin like giant Zeeman effect. These peculiar Zeeman splittings of the excitonic lines result from a highly nonlinear heating of Mn spins by injected hot photocarriers. At low magnetic field, Mn spins are driven out of equilibrium by the carriers, whereas, above a critical magnetic field B_c, the thermal equilibrium of Mn spins with the lattice is almost restored. We will study how this critical field B_c, at which this abrupt transition occurs, depends on the lattice temperature, the density of the injected carriers and the Mn concentration. Especially, B_c is expected to be almost zero for high Mn concentrations (typically above 4%) and too high to be observable in the extremely diluted case (well below 1%). It may explain why this nonlinear behavior has never been observed yet in magnetic QDs.

The organization of the paper is as follows: In Sec. II, we give experimental details about samples and optical spectroscopy. In Sec. III, we present the experimental results and the theoretical model describing the dynamical equilibrium between Mn spins and photocarriers. In Sec. IV, we discuss the parameters of the model used to fit the data. Section V summarizes our results.

II. EXPERIMENTAL DETAILS

We performed microphotoluminescence (μ-PL) of single QDs under magnetic field in Faraday geometry. The two circular polarizations $\sigma^{\pm}$ are detected under cw nonresonant laser excitation (514 nm, i.e., 2411 meV). The μ-PL is excited through submicrometer apertures in Al masks deposited on top of the samples. The samples are placed in a helium cryostat under static magnetic field up to 11T applied parallel to the growth axis z. The samples contain a single plan of Cd(Mn)Te/ZnTe self assembled QDs grown by molecular beam epitaxy (MBE) on ZnTe substrates.[12] The deposition of 6 monolayers of Cd(Mn)Te gives rise to QDs of typically 3 nm height and 10 nm diameter, with a wetting layer of few monolayers.[13] In these QDs, we change the nominal Mn concentrations from $x_{\mathrm{Mn}}=1.5\%$ to 5.5%. The samples are nominally undoped and all carriers under consideration are photocreated ones.

In a magnetic QD, the typical magnetic field dependence of the exciton energy is given by the so called giant Zeeman effect.[14] Magnetic ions are paramagnetic and their average spin component along the z axis $\langle S_z\rangle$ is given by the modified Brillouin function:

$$\langle S_z\rangle = -5/2 B_{5/2}\left[\frac{5/2\cdot g_{\mathrm{Mn}}\mu_B B}{k(T_{\mathrm{Mn}}+T_0)}\right], \quad (1)$$

where $B_{5/2}(x)$ is the Brillouin function, T_0 is the effective temperature, which phenomenologically describes the anti-

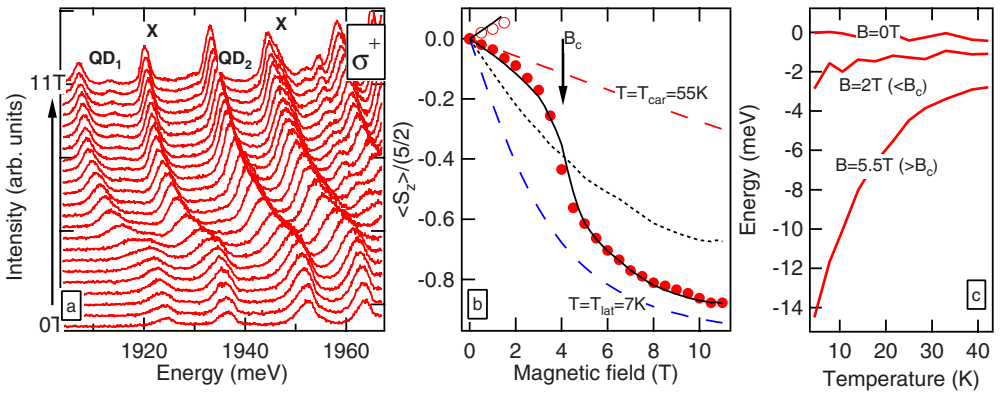

FIG. 1. (Color online) (a) μ-PL spectra of two Cd(Mn)Te QDs (QD_1 and QD_2) with $x_{Mn}=1.5\%$ at $T=7$ K and recorded in σ_+ polarization. For each dots excitonic lines (labeled by X) are plotted from $B=0$ T to 11 T; The two lines shifted by 11 meV toward low energy may correspond to biexcitonic lines or charged state of QD_1 and QD_2 (see text). The spectra are recorded every 0.5T. (b) Mn spin orientation $2/5\langle S_z\rangle$ obtained from the normalized energy shift of the excitonic line of QD_1 [see Eq. (2)] as a function of B at $T=7$ K for σ^+ (red solid circles) and σ^- (red open circles). The black solid line is the numerical calculation based on the model described in Sec. III B and performed with the following parameter set as defined in the text: $T_{lat}=7$ K, $T_{car}=55$ K, $1/T_1=2\times10^5$ s^{-1}, $n_{car}=8\times10^7$ cm^{-2}, $x_{Mn}=1.5\%$, $L_z=1.5$ nm and $\epsilon=0.8$ (holes). The blue and red dashed lines are two Brillouin functions at $T_{Mn}=7$ K and $T_{Mn}=55$ K, respectively. The arrow indicates the transition from hot to cold at $B_c=4$ T (defined by the inflexion point). The black dotted line is a numerical calculation assuming constant flip-flop transitions probabilities $W_k^{\pm}$ and a magnetic field dependent spin-lattice relaxation T_1 [see Fig. 2(c) and Sec. IV B]. (c) Excitonic Zeeman shift of QD_1 plotted as function of the lattice temperature for 3 different magnetic fields below (0 and 2 T) and above (5.5 T) B_c. The Zeeman shifts have been corrected from the few meV redshift due the band-gap variation with temperature.

ferromagnetic Mn-Mn exchange interaction,[15] $g_{Mn}=2$ is the g factor of the Mn d electrons and T_{Mn} is the Mn spin temperature. Taking into account the sp-d exchange interactions, the expected $\sigma\pm$ exciton energy shifts become

$$E_X^{\sigma^\pm}(B)-E_X^{\sigma^\pm}(B=0)=\pm\Delta E_{QD}^{\mathrm{sat}}\frac{\langle S_z\rangle}{5/2}, \qquad (2)$$

where $\Delta E_{QD}^{\mathrm{sat}}$ is the giant Zeeman shift at saturation. $\Delta E_{QD}^{\mathrm{sat}}$ depends on the effective Mn concentration in the vicinity of the dot,[15] on the sp-d exchange integrals and on the shape of the envelop functions of electrons and holes.[16] This formulation,[16] where the Zeeman shift is proportional to an effective Mn concentration and to a saturated spin projection $\langle S_z\rangle=5/2$ is equivalent to the formulation where the Zeeman shift is proportional to the real Mn concentration and to an effective spin projection at saturation $\langle S_z\rangle=S_{\mathrm{eff}}$.

III. RESULTS

A. Experimental data

Figure 1(a) shows a series of (μ-PL) spectra recorded at $T=7$ K and at different magnetic fields for a sample with a Mn concentration of 1.5%. The intensity of the two lines labeled by X have a linear dependence with the excitation power and we ascribed them to the excitonic lines of two individual QDs (QD_1 and QD_2). The two other lines have the same behavior under magnetic field. They are about 11 meV below the excitonic lines and their intensities have a superlinear dependence with the excitation power (typically $\propto P^{1.4}$). These properties seem to indicate that they correspond to biexcitonic lines.[17] Their intensity decrease in σ_- polarization similarly to X lines, which is not expected for biexcitons and they may rather correspond to charged state of QD_1 and QD_2. These lines are not considered in the following.

Excitonic linewidths are typically 4 meV at $B=0$ T and 2 meV at $B=11$ T. These linewidths are in good agreement with the theoretical expectations for line broadening due to the thermal fluctuations of a finite number of independent Mn located in the QD.[16,18–20] Moreover, the linewidth decreases with magnetic field proportionally to the mean square deviation of the spin polarization ($\Delta S_z=[\langle S_z^2\rangle-\langle S_z\rangle^2]^{1/2}$), which decreases at $T=7$ K of about a factor 2 between 0 and 11 T.

Figure 1(b) shows the energy shift of the excitonic line of QD_1 in σ_+ and in σ_- polarizations. This shift has been normalized to the value at saturation $\Delta E_X^{sat}=17$ meV and is proportional to the normalized Mn spin polarization $2/5\langle S_z\rangle$ according to Eq. (2). Both excitonic lines of QD_1 and QD_2 undergo the same energy shift, which strongly deviates from the Brillouin like giant Zeeman effect. This shift is smaller than expected at low field, undergoes a steep transition at a critical field of about $B_c=4$ T and finally smoothly reaches the usual saturation above 4 T (B_c is defined by the inflexion point of excitonic Zeeman shift curve). In σ_- polarization, the excitonic lines follow a symmetric energy shift toward high energy. The intensities of these lines decrease as a function of magnetic field so that they cannot be observed anymore above 2 T.

According to Eq. (2), the exciton energy shift is a probe of Mn spin orientation $\langle S_z\rangle$ and consequently of Mn spin temperature [Eq. (1)]. Below the transition field B_c, data are in good agreement with a Brillouin function calculated for $T_{Mn}=55$ K corresponding to the photocarrier effective temperature (see Sec. III B). Above B_c, the data tend to reach a Brillouin function calculated for $T_{Mn}=7$ K corresponding to the lattice temperature (at high field, the small difference

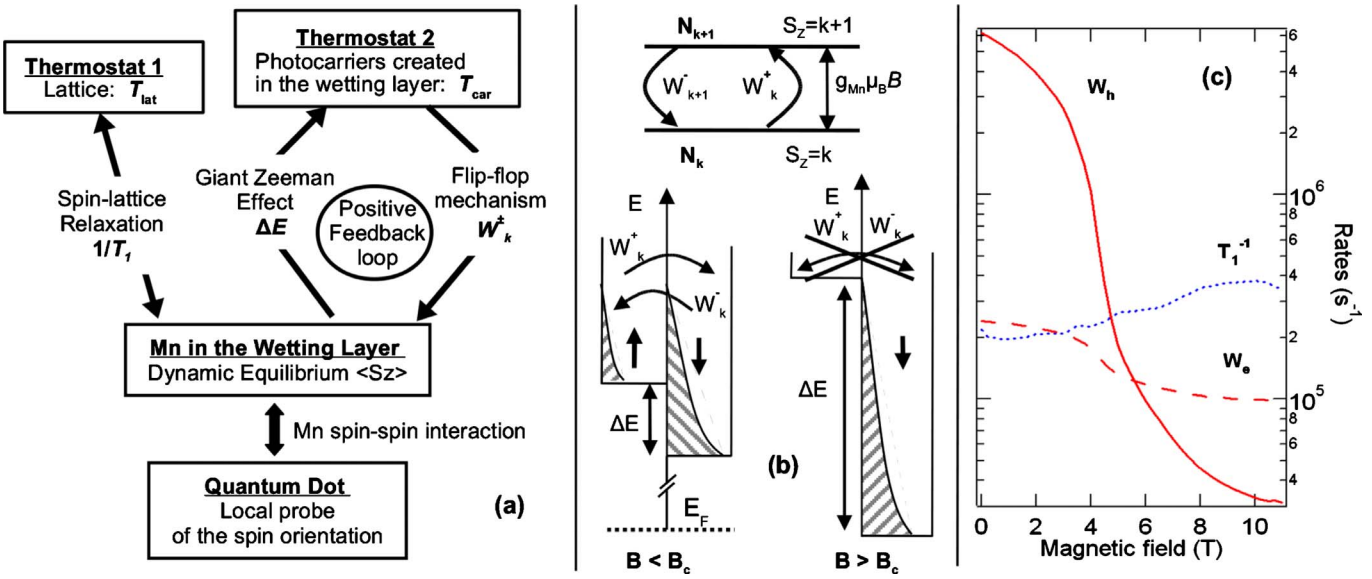

FIG. 2. (Color online) (a) Scheme of the interactions at stakes in the system. Mn spins interact with two thermostats: the lattice and the photocarriers. The QD acts as a local probes of the magnetic order; (b) Top: Two of the six Zeeman levels of a 5/2 Mn spin under a magnetic field $B>0$. $W_k^{\pm}$ are the transition probabilities between two levels due to flip-flops with photocarriers. Bottom: Density of occupied states for the 2D photocreated carrier gas and principle of the spin heating process. For $B<B_c$, mutual spin flips of carriers with Mn are allowed. But for $B>B_c$ the flip-flop mechanism is forbidden and the heating process is switched off; (c) Averaged flip-flop transition probabilities $W_{e,h}$ defined in Sec. IV B and spin lattice relaxation rate T_1^{-1} estimated from Ref. 31 for $x_{Mn}=1.5\%$ (blue dotted line) plotted as function as magnetic field. The red solid line shows W_h calculated for holes with the parameter set given in Fig. 1 and $J=\beta$. The red dashed line shows W_e calculated for electrons with the parameters given in caption of Fig. 1, $\epsilon=1$ and $J=\alpha$ (see Sec. IV B).

between the data and the Brillouin function is discussed in Sec. IV B). Mn spins are hot below B_c and cold above. Thus we have a magnetic field dependent thermal equilibrium of Mn spins with a steep transition from the hot to the cold regime.

Another way to reveal the anomalous behavior of the Mn temperature is to study the temperature dependence of the excitonic Zeeman shift for given magnetic fields [see Fig. 1(c)]. The Zeeman shifts have been corrected from the few meV redshift due the band gap variation with temperature. Below B_c ($B=2$ T), we observed a small blue shift with the lattice temperature because the Mn temperature is mainly controlled by the photocarrier one ($T_{car}=55$ K). By contrast, above B_c ($B=5.5$ T) the Mn temperature increases with the lattice one following a Brillouin like behavior [see Fig. 1(c)].

B. Model

In previous works on concentrated magnetic QDs (typically above 7%), deviations from Brillouin like giant Zeeman effect have been observed and attributed to the formation of the magnetic polaron (MP) [i.e., partial orientation of Mn spins in the exchange field of zero-dimensional (0D) photocarrier located in the QDs].[21,22] The behavior observed here cannot be attributed to the formation of MP because it should present a strong blue shift at zero magnetic field as the lattice temperature increases.[21] Such effect is not observed in our case [see Fig. 1(c)]. Moreover, no energy shift has been observed in the single dot time resolved photoluminescence, which would have been a fingerprint of the MP formation time. Furthermore, from theoretical point of view the MP formation is rather unlikely in the low Mn concentrated QDs studied here.[23]

To explain the experimental results, we consider that Mn spins, randomly distributed in the QDs and in the WL, are heated by hot photocarriers generated by the non resonant laser excitation. To describe Mn spin dynamics, we take into account the spin lattice interaction and the spin carrier flip-flop mechanisms. The relevant time scale of these processes are typically in the microsecond range [see Fig. 2(c)]. As a consequence, the Mn spin distribution is expected to be the same in the WL and in the QD due to faster spin-spin interaction and spin diffusion processes.[10,24] In this picture the QD acts as a local probe of the Mn spin orientation, which results from the simultaneous interaction of Mn with two thermostats [see Fig. 2(a)]. The first one is the lattice at a temperature T_{lat}, which interacts with Mn at a rate T_1^{-1} where T_1 is the spin-lattice relaxation time.[25] The second one is composed by the hot photocarriers generated in the WL, described as a Fermi-distributed 2D carrier gas at a temperature T_{car}. The coupling between Mn spins in the wetting layer and photocarriers results from mutual flip-flop mechanisms. Its magnetic dependence is due to the giant Zeeman splitting of the photocarrier spin subbands, which spin polarizes the photocarriers at high magnetic field [see Figs. 2(a) and 2(b)]. Consequently, the steady state of Mn spins results from a dynamic equilibrium with two thermostats.

For 0D carriers confined on discrete levels in the QD, flip-flop mechanisms with Mn spins are forbidden because the energy conservation cannot be fulfilled when the levels are split by a giant Zeeman splitting much larger than the Mn Zeeman energy. They do not participate to the Mn heating process.

The behavior of the system can be well understood within a few qualitative arguments. First, looking at Fig. 2(b), one can understand why Mn are only heated at low-magnetic field: mutual spin flips between Mn and 2D carriers are allowed and give rise to an energy transfer from hot carriers to Mn spins. For example, a transition from spin up to spin down subband for photocarriers leads to a transition from S_z to S_z+1 for Mn spins [see Fig. 2(b)]. At sufficiently high B, the giant Zeeman splitting ΔE is large enough to polarize almost completely the 2D carriers. As the magnetic field increases, the Mn Zeeman energy becomes smaller than the spin splitting ΔE: mutual spin flips are blocked and the heating process is switched off. The Mn-carrier interaction is thus, modulated by B.

The steepness of the transition from hot to cold at B_c is explained by the existence of a positive feedback loop between Mn and 2D carriers. As the Mn orientation $\langle S_z \rangle$ increases, the splitting ΔE and the polarization of the 2D carriers increase. In return a reduced heating of the Mn system occurs due to a decreasing number of flip-flop events; this induces a further increase in the initial Mn orientation $\langle S_z \rangle$. Without such feedback loop in the Mn heating process, the calculated transition from the hot to the cold regime is always smoother than the one observed experimentally.

This dynamic equilibrium is well described by the rate equations of the six Zeeman populations of Mn spins N_k and by finding numerically their stationary solutions:

$$\frac{\partial N_k}{\partial t} = -\frac{1}{T_1}(N_k - N_k^{\mathrm{eq}}) + W_{k+1}^{-}N_{k+1} + W_{k-1}^{+}N_{k-1} - W_k^{-}N_k - W_k^{+}N_k \quad \text{for} \quad k = S_z = \pm\frac{5}{2}, \pm\frac{3}{2}, \pm\frac{1}{2}. \tag{3}$$

The first term of the right hand side describes the interaction with the lattice [Fig. 2(a)]. N_k^{eq} is the thermal equilibrium value of N_k, which causes $\langle S_z \rangle$ to be equal to a Brillouin function at $T_{\mathrm{Mn}}=T_{\mathrm{lat}}$ when only considering the lattice thermostat. All the other terms of the right hand side depending on $W_k^{\pm}$ describe the interaction with the photocarrier reservoir. $W_k^{\pm}$ are the transition probabilities between two Zeeman levels of Mn spins [Figs. 2(b) and 2(c)]. They account for the flip-flop mechanism between Mn spins and 2D carrier spins which are created in the WL, described as an infinitely deep 2D QW. This mechanism is due to the dynamic part of the *sp-d* exchange Hamiltonian between Mn and 2D photocreated carriers:[8,11,26]

$$H_{sp-d} = \sum_{\vec{R_i}} J\delta(\vec{r} - \vec{R_i})\left[\sigma_z S_z + \epsilon\frac{1}{2}(\sigma_+ S_- + \sigma_- S_+)\right], \tag{4}$$

where $\vec{S}$, $\vec{\sigma}$ are the spin operators for Mn and carriers, respectively, J is the exchange integral ($J=\alpha$ for electrons and $J=\beta$ for holes), $\vec{R_i}$ are the coordinates of Mn ions. In the Hamiltonian, the first term gives rise to the giant Zeeman splitting ΔE in the WL [see Fig. 2(b)], whereas the second one describes the flip-flop mechanisms between photocarriers and Mn. ΔE at saturation is proportional to the effective Mn composition calculated from x_{Mn} using Ref. 27. The rate equations are solved by taking into account simultaneously both type of carriers. For electrons, the spin is isotropic so $\epsilon=1$. For holes, we introduce an effective parameter $0<\epsilon<1$ describing the valence band mixing between light holes and heavy holes in the wetting layer.[28,29] For electrons and holes, $W_k^{\pm}$ can be derived from the Fermi golden rule using Eq. (4):

$$W_k^{+} = a_k\frac{3\pi}{\hbar}\epsilon^2 J^2\left(\frac{D}{L_z}\right)^2 kT_{\mathrm{car}}\frac{\ln(x_1+x_2)-\ln(1+x_2)}{x_1-1},$$

$$\text{where} \quad x_1 = \exp\left(\frac{g_{\mathrm{Mn}}\mu_B B}{kT_{\mathrm{car}}}\right), \quad x_2 = \exp\left(\frac{\Delta E/2 - E_f}{kT_{\mathrm{car}}}\right), \tag{5}$$

$$W_{k+1}^{-} = W_k^{+}\exp\left(+\frac{g_{\mathrm{Mn}}\mu_B B}{kT_{\mathrm{car}}}\right), \tag{6}$$

where $k=-5/2, \pm 3/2, \pm 1/2$ and a_k numerical coefficients: $a_{-5/2}=a_{3/2}=5/4$, $a_{-3/2}=a_{1/2}=2$, $a_{-1/2}=9/4$. L_z is the WL width, $D=\frac{m_{\mathrm{car}}^*}{2\pi\hbar^2}$ is the density of states for one spin subband of the WL ($m_{\mathrm{car}}^*=0.1m_0$ for electrons, $m_{\mathrm{car}}^*=0.25m_0$ for holes where m_0 is the free electron mass). T_{car} is the temperature of the carrier gas and E_f its Fermi energy:

$$E_f = kT_{\mathrm{car}}\ln\left(\sqrt{\cosh^2\left(\frac{\Delta E}{2kT_{\mathrm{car}}}\right) + \exp\left(\frac{n_{\mathrm{car}}/D}{kT_{\mathrm{car}}}\right) - 1} - \cosh\left(\frac{\Delta E}{2kT_{\mathrm{car}}}\right)\right), \tag{7}$$

n_{car} is the carrier density generated in the WL. For low densities, E_f is located in the band gap and the Fermi distributions look like Boltzmann ones [see Fig. 2(b)]. ΔE is the giant Zeeman splitting between the two carrier spin subbands (electron or hole) [see Fig. 2(b)]. In Eq. (6), the ratio of W_k^{+} to W_{k+1}^{-} is equal to $\exp(-\frac{g_{\mathrm{Mn}}\mu_B B}{kT_{\mathrm{car}}})$. Let's note that the photocarriers behaves as a real thermostat at T_{car}. Thus the Mn average spin $\langle S_z \rangle$ follows a Brillouin function at $T=T_{\mathrm{car}}$ when only considering the carrier thermostat. Taking into account the energy conservation during flip-flop processes requires a complete derivation of $W_k^{\pm}$. We perform such a derivation by contrast with previous works.[8,11]

C. Sensitivity to the experimental parameters

The dynamic equilibrium of Mn can be seen as an effective Mn spin temperature which is the average of T_{lat} and T_{car} weighted by the spin flip rates T_1^{-1} and $W_k^{\pm}$ respectively. Because $W_k^{\pm}$ decrease while increasing B [Fig. 2(c)], this effective temperature goes from T_{car} to T_{lat} approximatively [Fig. 1(b)]. The switching from the hot to the cold regime results from the crossing between the flip-flop transition probabilities ($W_k^{\pm}$) and the spin lattice relaxation rate $1/T_1$ [see Fig. 2(c)]. The decrease of $W_k^{\pm}$ results from the rising polarization of the carrier gas [Fig. 2(b)]. This polarization can be essentially controlled by three variables; the lattice temperature T_{lat}, the photocarrier density n_{car} and the Mn concentration x_{Mn}. We performed experiments by changing intentionally

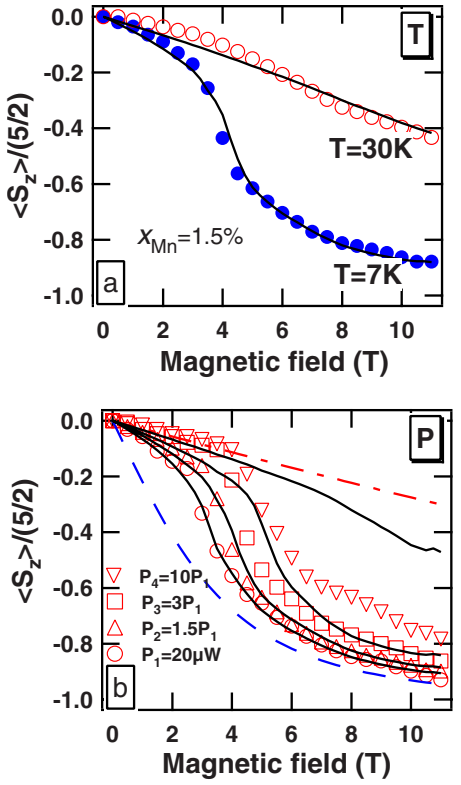

FIG. 3. (Color online) The red and blue symbols correspond to experimental data and the solid black lines to numerical calculations. (a) B dependency of $2/5\langle S_z\rangle$ for two cryostat temperatures $T=7$ K [same data than in Fig. 1(b)], $T=30$ K (solid blue and open red circles, respectively) Both spectra have been taken with an excitation power of 32 μW. The fitting parameters at $T=30$ K are equal to the ones at $T=7$ K [see Fig. 1(b)], except T_{car} equal to 80 K. (b) B dependency of $2/5\langle S_z\rangle$ at $T=7$ K for different laser powers P. We use the parameter set given in the caption of Fig. 1(b) and we change only the carrier density $n_{car}=0.5,0.75,1.5,5\times10^8$ cm^{-2} (from top to bottom), proportionally to the excitation power. Blue dashed and red dash-dotted lines are two Brillouin functions at $T_{Mn}=7$ and 55 K, respectively.

these 3 key parameters (see Figs. 3 and 4). A quantitative agreement between the calculation (solid lines) and the data (symbols) is obtained for all experimental data performed at low power. The detail of the parameter set used in the model is described in Sec. IV B.

Figure 3(a) shows the exciton Zeeman shift in σ_+ polarization of QD_1 (1.5% sample) for two cryostat temperatures. The transition is less abrupt at $T=30$ K (which corresponds to T_{lat}) than for $T=7$ K [same data as shown in Fig. 1(b)]. Since T is higher, the effective Mn temperature is higher and the variation of the Zeeman shift with magnetic field is softened. Figure 3(b) shows the exciton Zeeman shift in σ_+ polarization of QD_1 at $T=7$ K for different excitation powers. Since, the carrier density n_{car} is proportional to the excitation power P, B_c rises with P. Indeed, the higher the carrier density, the more difficult it is to polarize them. As discussed in Sec. IV B for high-power densities, the calculated values of B_c are larger than the experimental ones.

Figure 4(a) and 4(b) show a series of μ-PL spectra of single QD for samples containing a larger Mn concentration (respectively, 3.5% and 5.5%). The spectra have been recorded at 7 K in σ_+ polarization for different magnetic fields between 0 and 11 T. The linewidth in zero field (respectively, 6 and 10 meV) increases as expected with the Mn concentration. In Fig. 4(c), we show the magnetic field dependence of the excitonic Zeeman shift for single dots of the different samples. The reported giant Zeeman shifts are normalized by $\Delta E_X^{sat}=33$ meV for $x_{Mn}=3.5\%$ and by $\Delta E_X^{sat}=38$ meV for $x_{Mn}=5.5\%$. We observe that B_c decreases when x_{Mn} increases. The higher x_{Mn}, the higher ΔE, so that the carriers are immediately polarized at low magnetic fields [see Fig. 2(b)] and B_c is almost zero. By contrast, for very low x_{Mn} (not shown here), carriers are never completely polarized and B_c is very large (B_c is infinite in the limit of a single Mn ion, see Ref. 1). This qualitative description corresponds in the model to the decrease in the flip-flop transition probabilities ($W_k^{\pm}$) with magnetic field [see Fig. 2(c)]. As a consequence, only a small range of Mn concentrations allows observing the transition from hot to cold regimes.

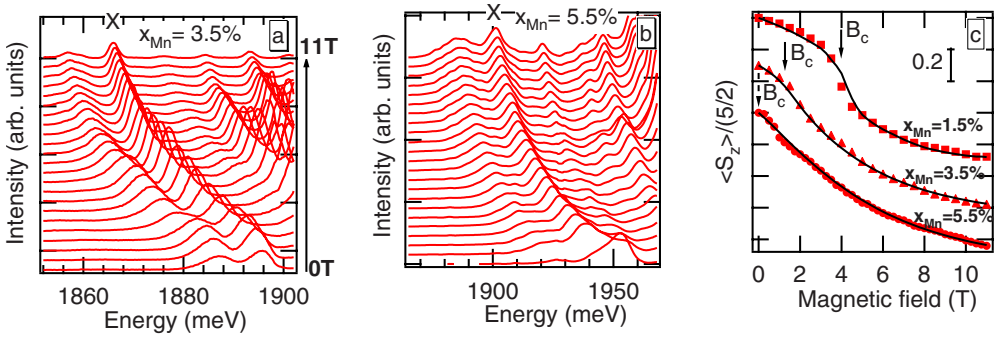

FIG. 4. (Color online) (a) μ-PL spectra of a Cd(Mn)Te QD with a nominal Mn concentration $x_{Mn}=3.5\%$ recorded at $T=7$ K in σ_+ polarization. Excitonic lines of individual QDs (labeled by X) are plotted from $B=0$ T to 11 T; The spectra are recorded every 0.5 T. (b) μ-PL spectra of a Cd(Mn)Te QD with a nominal Mn concentration $x_{Mn}=5.5\%$ recorded at $T=7$ K in σ_+ polarization. Excitonic lines are plotted from $B=0$ to 11 T. All spectra have been taken with a low power excitation. (c) magnetic field dependence of $2/5\langle S_z\rangle$ at $T=7$ K for different Mn concentration x_{Mn}. The curves have been arbitrarily shifted of 0.2 for enhanced visibility. The calculations (solid lines) have been obtained with the parameter set given in the caption of Fig. 1(b) except for T_{lat} and $1/T_1$: $T_{lat}=10$ K and $1/T_1=10^6$ s^{-1} for $x_{Mn}=3.5\%$, $T_{lat}=12$ K and $1/T_1=9\times10^6$ s^{-1} for $x_{Mn}=5.5\%$ (see text).

IV. DISCUSSION

A. Main features of the model

A similar model has been developed for quantum wells in Ref. 11 using an analytical approach. By contrast with the latter, the model presented in this paper allows (i) to describe the Mn dynamics even when the temperature difference between the two thermostats is large and (ii) to explicitly account for the energy conservation during flip-flop events. These improvements have been performed at the expense of a numerical resolution of the rate equations. It has to be also mentioned that, we did not take into account an eventual out of equilibrium spin distribution of the photocarriers.[11] It could be incorporated within our calculations without changing the physical interpretation of the data and the main conclusions of this paper.

B. Parameters of the model

We will finally discuss the parameters of the model. It is interesting to note that numerical calculations account for all data with a single set of parameters. Among the seven parameters [see caption of Fig. 1(b)] used in the model, four of them were estimated from experimental features, T_{lat} from the cryostat temperature T, T_1^{-1} from literature, x_{Mn} and L_z from molecular beam epitaxy informations. Let's note that in the different samples the QD's excitonic shifts at saturation are in good agreement with the nominal Mn concentration determined by MBE. The three other ones, T_{car}, n_{car} and ϵ were used as fitting parameters in the numerical calculations.

In all fits, the lattice temperature T_{lat} has been taken equal to the cryostat temperature T except for high Mn concentrations: For $x_{\mathrm{Mn}}=3.5\%(5.5\%)$, we had to take respectively $T_{\mathrm{lat}}=10$ K (12 K) for a cryostat temperature of 7 K. This difference could be explained by an indirect Mn heating by phonons generated by the non resonant excitation.[30,31] This small increase in the lattice temperature plays a minor role in the abrupt transition induced by the direct heating underlined in this work (flip-flop mechanism with carriers).

The dependence of T_1 on x_{Mn}, T_{lat}, and B has been estimated interpolating data of literature.[25,32,33] The increase of $1/T_1$ with x_{Mn} (see caption of Fig. 4) contributes to the low value of B_c for the high Mn concentration. Following reference,[33] T_1^{-1} rises with magnetic field due to the influence of the phonon density of states [see Fig. 2(c)]. However, we cannot fit the experimental data assuming a constant spin heating rate $W_k^{\pm}$ and an increasing T_1^{-1} with magnetic field [see dotted line in Fig. 1(b)]. This highlights the necessity to take into account magnetic field dependant flip-flop transition probabilities. $W_k^{\pm}$ are also proportional to L_z^{-2} [Eq. (5)]. Due to more confined carrier wave functions, $W_k^{\pm}$ is enhanced as we reduce the system dimensions[11] i.e., from quantum wells (Ref. 11) to very thin 2D wetting layers (this work).

The parameter T_{car} is determined by fitting the data before B_c with a Brillouin function. It has been found as high as 55 K. This value is higher than the reported value in previous works, but one has to consider that we used a μ-PL setup, which generates high excitation power densities typically 100 times higher than the ones used in macro-PL setups.[11] For the measurements performed with a cryostat temperature $T=30$ K, we found a larger carrier temperature $T_{\mathrm{car}}=80$ K. This may result from a lower efficiency of the electron-phonon processes, which relax the energy of hot carriers in the wetting layer.

The parameter n_{car} results from a fit of the data obtained at low excitation power. There is a good agreement for n_{car} varying from 5×10^7 to 8×10^7 cm^{-2} [see Figs. 1(b) and 3]. For higher excitation powers [Fig. 3(b)], n_{car} was adjusted according to the variation in the excitation power. In agreement with the experiment, B_c increases with the excitation power. However, the calculated values of B_c are larger than the experimental ones for $P\geq60$ μW.

With low-photocarrier densities of about 10^7 cm^{-2}, the 2D density of states of the WL, which parametrizes the flip-flop transition probabilities, is surely modified by disorder. However, we would like to emphasize that the flip-flop mechanisms between Mn and photocarriers are not suppressed by disorder providing that (i) a quasi-continuum of density of states remains in the WL in order to fulfill the conservation of Zeeman energy, and (ii) the bands are populated by out of equilibrium carrier distributions, not necessary described by an effective carrier temperature. A complete calculation would require to replace the flip-flop transition probabilities $W_k^{\pm}$ given by Eq. (5) by expressions taking into account disorder modified density of states and non Boltzmann carrier distributions. Moreover, the two thermostats (phonons bath and photocarriers) are not independent of each other. The coupling between them has not a direct influence as long as they behave as thermostats characterized by two different temperatures. This description may become inadequate at high excitation power. In that case a more complete model describing the dynamical equilibrium between photocarriers, phonons, laser excitation and Mn spins has to be considered. Such a model is beyond the scope of this paper dedicated to the low excitation power conditions. We just demonstrate here that the coupling between photocarriers and Mn in the WL can account consistently (i.e., with a reasonable set of parameters) for the abruptness of the experimental hot to cold transition under magnetic field. This justifies why we performed a calculation using a restrictive assumption such as a 2D Fermi gas.

The last free parameter is ϵ, which parametrizes the flip-flop transition probabilities $W_k^{\pm}$. Figure 2(c) shows the magnetic field dependence of averaged values of $W_k^{\pm}$, defined for electron and holes by

$$W_{e,h}=\frac{W_k^{+}+W_{k+1}^{-}}{a_k}. \tag{8}$$

They are calculated for electrons and holes with the parameter set given in the caption of Fig. 1 and compared with the spin lattice relaxation rate T_1^{-1} estimated for $x_{\mathrm{Mn}}=1.5\%$ using data of Ref. 33. For electrons, $\epsilon=1$, $J=\alpha$ with $N_0\alpha=220$ meV (Refs. 14 and 15) and the variation of $W_k^{\pm}$ is not large enough to explain the transition from a hot regime to a cold one. By contrast, for holes ϵ is a fitting parameter and we found $\epsilon=0.8$. Using $J=\beta$ with $N_0\beta=-880$ meV,[14,15] ΔE

is large enough to create a great variation of $W_k^{\pm}$ on a small range of magnetic fields, due to the positive feedback loop [see Fig. 2(c)]. Holes are thus responsible for the transition from a hot to a cold regime, while electrons mainly induce a constant spin heating effect, independent of magnetic field. A signature of this constant heating can be seen on Fig. 1(b) above B_c, where the fit is not superposed with the cold Brillouin function. Numerical calculations demonstrate the important role played by holes in the heating process through a nonzero value of ϵ, which corresponds to a heavy-light hole mixing (induced by strain inhomogeneities in the WL). The large value of ϵ taken in our model might describe the multiple flip-flops of one hole with several Mn spins.[34]

Finally let's note that the critical magnetic field B_c, defined by the crossing between the flip-flop transition probabilities and the spin lattice relaxation rate, can only be observed for specific conditions of nonresonant excitation powers and Mn concentrations.

V. CONCLUSION

In conclusion, single QDs can act as a very sensitive probe of Mn orientation: we observed a dynamic equilibrium of Mn spins, which results from a highly nonlinear spin heating process. This process is well described by a positive feedback loop (modulated by B) with photocarriers created in the WL underneath QDs. It appears this direct heating is mainly provided by holes. This nonlinear effect is crucial for nanometer-sized quantum systems. First the small size strongly increases the Mn-carrier interaction. Second the number of Mn at stakes is limited: when dealing with only few Mn, namely for Mn concentration between 1 and 4% the direct heating is the preponderant mechanism. For instance in the ultimate limit, a single Mn spin is constantly heated by surrounding carriers. This demonstrates the great importance to control the QD coupling with its local environment in order to manipulate few Mn spins in QDs.

ACKNOWLEDGMENTS

We would like to thank J. Cibert for fruitful discussions. This work was supported by French A.N.R contract CoSin.

*david.ferrand@grenoble.cnrs.fr

[1] L. Besombes, Y. Léger, L. Maingault, D. Ferrand, H. Mariette, and J. Cibert, Phys. Rev. Lett. **93**, 207403 (2004).
[2] A. Kudelski, A. Lemaître, A. Miard, P. Voisin, T. C. M. Graham, R. J. Warburton, and O. Krebs, Phys. Rev. Lett. **99**, 247209 (2007).
[3] A. O. Govorov, Phys. Rev. B **70**, 035321 (2004).
[4] J. Fernández-Rossier, Phys. Rev. B **73**, 045301 (2006).
[5] A. Berthelot, I. Favero, G. Cassabois, C. Voisin, C. Delalande, Ph. Roussignol, R. Ferreira, and J. M. Gérard, Nat. Phys. **2**, 759 (2006).
[6] L. Besombes, Y. Léger, J. Bernos, H. Boukari, H. Mariette, J. P. Poizat, T. Clément, J. Fernandez-Rossier, and R. Aguado, Phys. Rev. B **78**, 125324 (2008).
[7] V. D. Kulakovskii, M. G. Tyazhlov, A. I. Filin, D. R. Yakovlev, A. Waag, and G. Landwehr, Phys. Rev. B **54**, R8333 (1996).
[8] M. G. Tyazhlov, A. I. Filin, A. V. Larionov, V. D. Kulakovskii, D. R. Yakovlev, A. Waag, and G. Landwehr, Sov. Phys. JETP **85**, 784 (1997).
[9] F. Teppe, M. Vladimirova, D. Scalbert, T. Wojtowicz, and J. Kossut, Phys. Rev. B **67**, 033304 (2003).
[10] M. Vladimirova, D. Scalbert, and C. Misbah, Phys. Rev. B **71**, 233203 (2005).
[11] B. König, I. A. Merkulov, D. R. Yakovlev, W. Ossau, S. M. Ryabchenko, M. Kutrowski, T. Wojtowicz, G. Karczewski, and J. Kossut, Phys. Rev. B **61**, 16870 (2000).
[12] L. Maingault, L. Besombes, Y. Léger, C. Bougerol, and H. Mariette, Appl. Phys. Lett. **89**, 193109 (2006).
[13] F. Tinjod, B. Gilles, S. Moehl, K. Kheng, and H. Mariette, Appl. Phys. Lett. **82**, 4340 (2003).
[14] J. K. Furdyna, J. Appl. Phys. **64**, R29 (1988).
[15] J. A. Gaj, R. Planel, and G. Fishman, Solid State Commun. **29**, 435 (1979).
[16] A. Hundt, J. Puls, and F. Henneberger, Phys. Rev. B **69**, 121309(R) (2004).
[17] L. Besombes, K. Kheng, L. Marsal, and H. Mariette, Phys. Rev. B **65**, 121314(R) (2002).
[18] R. Brazis and J. Kossut, Solid State Commun. **122**, 73 (2002).
[19] G. Bacher, A. A. Maksimov, H. Schömig, V. D. Kulakovskii, M. K. Welsch, A. Forchel, P. S. Dorozhkin, A. V. Chernenko, S. Lee, M. Dobrowolska, and J. K. Furdyna, Phys. Rev. Lett. **89**, 127201 (2002).
[20] Following Ref. 16, the ratio between the full width at half maximum (FWHM) of the zero field PL line and the Zeeman shift at saturation can be estimated from $FWHM/\Delta E_{QD}^{\mathrm{sat}}=2\sqrt{2\ln(2)}\times 2/5\times\sqrt{35/12}/\sqrt{N_{\mathrm{Mn}}}$ where N_{Mn} is the number of isolated Mn spins in the QD. Using $\Delta E_{QD}^{\mathrm{sat}}=17$ meV and FWHM=4 meV, we obtain $N_{\mathrm{Mn}}=46$ in agreement with the effective Mn concentration and QDs volume. Note that here the QD volumes are about 15 times larger than the ones in Ref. 16.
[21] A. A. Maksimov, G. Bacher, A. McDonald, V. D. Kulakovskii, A. Forchel, C. R. Becker, G. Landwehr, and L. W. Molenkamp, Phys. Rev. B **62**, R7767 (2000).
[22] J. Seufert, G. Bacher, M. Scheibner, A. Forchel, S. Lee, M. Dobrowolska, and J. K. Furdyna, Phys. Rev. Lett. **88**, 027402 (2001).
[23] C. Benoit à la Guillaume, Yu. G. Semenov, and M. Combescot, Phys. Rev. B **51**, 14124 (1995).
[24] A. A. Maksimov, *II-VI International Conference* (St. Petersburg, Russia, 2009).
[25] T. Dietl, P. Peyla, W. Grieshaber, and Y. Merle d'Aubigne, Phys. Rev. Lett. **74**, 474 (1995).
[26] V. S. Vikhnin, M. F. Deigen, Yu. G. Semenov, and B. D. Shanina, Sov. Phys. Solid State **18**, 1293 (1976).
[27] J. A. Gaj, W. Grieshaber, C. Bodin-Deshayes, J. Cibert, G. Feuillet, Y. Merle d'Aubigne, and A. Wasiela, Phys. Rev. B **50**, 5512

(1994).
[28] M. Tadić, F. M. Peeters, and K. L. Janssens, Phys. Rev. B **65**, 165333 (2002).
[29] Y. Léger, L. Besombes, L. Maingault, and H. Mariette, Phys. Rev. B **76**, 045331 (2007).
[30] M. K. Kneip, D. R. Yakovlev, M. Bayer, A. A. Maksimov, I. I. Tartakovskii, D. Keller, W. Ossau, L. W. Molenkamp, and A. Waag, Phys. Rev. B **73**, 035306 (2006).
[31] A. Hundt, J. Puls, A. V. Akimov, Y. H. Fan, and F. Henneberger, Phys. Rev. B **72**, 033304 (2005).
[32] D. Scalbert, J. Cernogora, and C. Benoît a la Guillaume, Solid State Commun. **66**, 571 (1988).
[33] T. Strutz, A. M. Witowski, and P. Wyder, Phys. Rev. Lett. **68**, 3912 (1992).
[34] A. V. Akimov, A. V. Scherbakov, D. R. Yakovlev, I. A. Merkulov, M. Bayer, A. Waag, and L. W. Molenkamp, Phys. Rev. B **73**, 165328 (2006).